DINAME 2017 - Proceedings of the XVII International Symposium on Dynamic Problems of Mechanics
A. T. Fleury, D. A. Rade, P. R. G. Kurka (Editors), ABCM, São Sebastião, SP, Brazil, March 5-10, 2017.

Distinguishing Rotating from Non-rotating Conditions in a Double Pendulum

Guilherme Luiz Torres Mendonça [1] **and Alberto Paiva** [1]

[1] Universidade Federal Fluminense – Volta Redonda School of Engineering – Department of Mechanical Engineering
420 Trabalhadores Av. – Volta Redonda − RJ – Brazil – 27.255-125
guilhermeid@hotmail.com, paiva.ufrj@gmail.com

Abstract: Elementary physical systems are often used to model practical mechanical applications; notwithstanding, despite of their simplicity, they may present complex nonlinear behaviors. Within this context, it is worthwhile to deeply understand their dynamical features, in order to explore all the richness of possible responses inherent to nonlinear systems. This paper concerns the numerical analysis of a double pendulum, based upon basins of attraction that enables the distinction between rotating and non-rotating conditions.

Keywords: Double pendulum, nonlinear dynamics, basin of attraction.

INTRODUCTION

In all science fields, the best solution not always is the most sophisticated. Sometimes, simple mechanical systems provide effective solutions with low cost. For instance, the pendulum rotating behavior may be exploited for energy harvesting (Nandakumar et al. 2012), as a mechanical *kinetic energy recovery system* (**KERS**). Despite of their apparent simplicity, pendulum systems play an outstanding role in practical applications due to their dynamical richness, inasmuch they are taken in their nonlinear form.

The study of nonlinear systems has evolved a lot in recently decades; however, much effort was devoted to low-dimensional dynamical systems that, nowadays, constitute a well-established subject in the literature. In order to illustrate how high-dimension systems may present more interesting phenomena, consider the fact that a typical one-degree of freedom system should be non-autonomous to present chaos, whereas systems with two or more degrees of freedom may present a chaotic response even for their natural behavior. The chaotic motion has a stochastic nature and some specific features are necessarily required for it to take place – notably, the system should be nonlinear and its dimension should be, at least, three. Besides that, it is well-known that nonlinear systems are sensitive to slight changes in both initial conditions and system parameters, which drastically affect their response, which may easily vary from periodic to chaotic and vice-versa. These high-dimension systems have been motivating innovative subjects such as: spatiotemporal chaos (Umberger et al. 1989; Awrejcewicz, 1991; Shibata, 1998; Lai & Grebogi, 1999; Kapitaniak, 2003; Machado et al. 2003; Ivancevic & Ivancevic, 2007; Sabarathinama et al. 2013, among others); synchronization phenomena (Buskirk & Jefries, 1985; Strogatz et al. 1989; Raj et al. 1999; Vincent & Kenfack, 2008; Ulrichs et al. 2009) and chimera investigation (Abrams & Strogatz, 2004; 2006; Kapitaniak, 2014; Martens, 2016).

Pendulum systems present a very particular characteristic – they may either oscillate around an equilibrium point or rotate about their pivoting joint, differing from other nonlinear oscillators that can only oscillate. Therefore, a variety of dynamical behaviors can take place, such as: period-1 or higher oscillations, period-1 or higher rotations, combined oscillation-rotations, besides more complex phenomena, such as chaos. Clearly, the oscillating behavior is associated with low energy levels, whereas the rotating one is related to high energy levels. This interesting dynamical versatility motivates some applications and, thus, stimulates the research interest in this subject. Wiercigroch and co-authors (Lenci et al. 2008; Nandakumar et al. 2012 and Najdecka et al. 2015) conducted numerical and experimental studies to evaluate the possibility of storing energy obtained from sea wave motion, which is responsible for a parametric excitation onto the pivoting joint, inducing a simple pendulum rotation. According to them, for an optimized energy harvesting, a stabilized period-1 rotating behavior is desirable. However, even for a stable rotation condition, other undesirable solutions may co-exist and compete with the rotating desired one. As a result, an active control strategy ends up necessary to keep a steady rotating behavior. Bishop et al. (1996); Bishop & Xu (1997) and De Paula et al. (2012; 2015) investigated control possibilities for a simple pendulum undergoing parametric excitation.

Specifically speaking about the double pendulum, it has been attracting the research community interest, as follows. Grebogi, Yorke and co-authors performed a coupled numerical–experimental study of chaos in a double pendulum using *Lyapunov* exponents (Shinbrot et al. 1992). Lankalapalli & Ghosal (1997) modeled the dynamical movement of arms and legs as double pendula to study chaos in a robot control, while Cross (2005, 2011) employed the same approach to describe human sporting activities. Rafat et al. (2009) analyzed the double pendulum dynamics with distributed mass. Stachowiak & Okada (2006) and Tang et al. (2011) investigated the chaos occurrence in a double

pendulum, while Szuminski (2014) studied the nonlinear dynamics (including chaos) of multiple pendula. Marszal et al. (2014) scrutinized the bifurcation phenomenon of both oscillatory and rotational solutions of a parametrically excited double pendulum. Heyl (2008), Elinson, J. (2013) and Small (2013) mapped the fractal structure presented by a double pendulum behavior, distinguishing rotating from non-rotating conditions.

This paper focuses on the numerical simulation of the double pendulum behavior, with the purpose of identifying the flip-over threshold for the rotation of either of both pendula, distinguishing rotating from non-rotating conditions. Besides that, the nature of these two conditions (periodic/chaotic) is investigated, through the evaluation of the Lyapunov exponents for some specific behaviors. The basins of attraction consider the natural conservative behavior by mapping the initial displacement conditions.

MATHEMATICAL MODELING

This section presents the dynamical equations of motion for the double pendulum, illustrated by the physical model presented in Fig. 1. θ_1 and θ_2 are the absolute angular displacements of the internal and external pendula, respectively taken with respect to inertial reference frame (x_1, x_2, x_3); L_1 and L_2 are the respective lengths of their rods; while m_1 and m_2 are their respective masses. The hypotheses adopted are: the rods are rigid and their masses are negligible compared with the bob masses m_1 and m_2; besides that, the system is submitted to gravitational body forces.

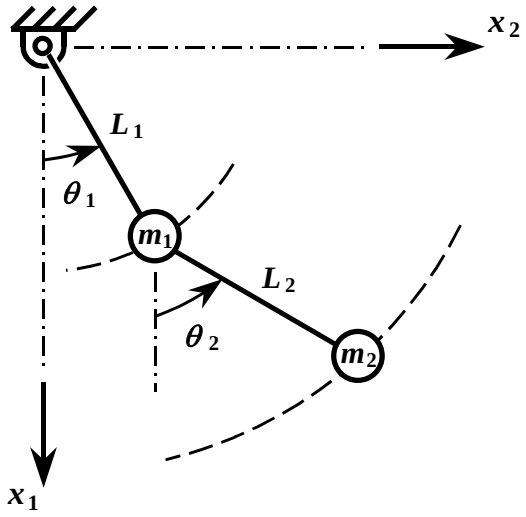

Figure 1 – Physical model for the double pendulum.

The mathematical formulation of the double pendulum may be found in several books (for instance: Santos, 2001) and, for the sake of conciseness, it is omitted here. Thereby, the set with the two homogeneous second-order ordinary differential equations, describing its natural behavior, is presented in Eq. (1), where $(\bullet)$ denotes the time derivative $d(\ )/dt$.

$$\begin{aligned} &\left(m_1+m_2\right)L_1\,\ddot{\theta}_1+m_2\,L_2\cos\left(\theta_2-\theta_1\right)\ddot{\theta}_2-m_2\,L_2\sin\left(\theta_2-\theta_1\right)\dot{\theta}_2^{\,2}+\left(m_1+m_2\right)g\sin\left(\theta_1\right)=0 \\ &m_2\,L_1\cos\left(\theta_2-\theta_1\right)\ddot{\theta}_1+m_2\,L_2\,\ddot{\theta}_2+m_2\,L_1\sin\left(\theta_2-\theta_1\right)\dot{\theta}_1^{\,2}+m_2\,g\sin\left(\theta_2\right)=0 \end{aligned} \tag{1}$$

For the purpose of numerical implementation, it is necessary to convert the original system consisting of two second-order ordinary differential equations into a new set of first-order ordinary differential equations with four equations. Hence, consider a variables' change, such that: $\theta_1=x$; $\dot{\theta}_1=y$; $\theta_2=w$ and $\dot{\theta}_2=z$.

$$\begin{cases} \dot{x}=y \\ \dot{y}=\dfrac{m_2\sin\left(w-x\right)\left[L_1\cos\left(w-x\right)y^2+L_2\,z^2\right]}{L_1\left[m_1+m_2\sin^2\left(w-x\right)\right]}+\dfrac{g\left[m_2\sin\left(2w-x\right)-\left(2m_1+m_2\right)\sin\left(x\right)\right]}{2\,L_1\left[m_1+m_2\sin^2\left(w-x\right)\right]} \\ \dot{w}=z \\ \dot{z}=-\dfrac{\sin\left(w-x\right)\left[\left(m_1+m_2\right)L_1\,y^2+m_2\,L_2\cos\left(w-x\right)w^2\right]}{L_2\left[m_1+m_2\sin^2\left(w-x\right)\right]}-\dfrac{g\left(m_1+m_2\right)\left[\sin\left(w-2x\right)+\sin\left(w\right)\right]}{2\,L_2\left[m_1+m_2\sin^2\left(w-x\right)\right]} \end{cases} \tag{2}$$

The algorithm for the basins of attraction generation was handmade conceived based upon a fourth-order Runge-Kutta method. For each set of initial conditions $\left(\theta_{10}, \theta_{20}, \dot{\theta}_{10}, \dot{\theta}_{20}\right)$, the displacement responses θ_{10} and θ_{20} are monitored to check whether any of them flips-over. When they reach this condition, the iteration time for this to occur is stored and associated with the values of the respective initial conditions. This procedure is repeated iteratively in order to cover the desired range of initial conditions. Eventually, in the own graphic generator software, a color scale is fitted to the iteration time range, considering the smallest and the greatest (no flip-over) values for this time iteration, providing the colormap displays.

NUMERICAL RESULTS

This section shows the numerical results considering the free response of the double pendulum mathematical model presented in the previous section. Concerning the dynamical system parameters, the acceleration due to gravity is assumed as g = 9.81 m/s^2, while masses m_1 and m_2 and rod lengths L_1 and L_2 will be varied during the simulations and their values will be indicated in each figure accordingly.

Initially, a reference condition is adopted, in order to verify the numerical code by comparison with existing results in the literature. A kinetic energy analysis, based on this reference condition, is conducted, to identify the most interesting initial conditions. Then, three analyses are performed, in order to distinguish rotating from non-rotating conditions in the double pendulum. At first, basins of attraction mapping initial displacement conditions (initial velocity conditions are null) are obtained, varying the value of a specific parameter (m_1, m_2, L_1 or L_2), while the others are kept constant. This analysis enables the identification of two contrasting situations – one of them preferably favoring the pendulum rotation and another one preferably inhibiting the pendulum rotation. Afterwards, based on these two situations, combinations of two varied parameters are simulated, aiming a better comprehension of these two distinct behaviors. At last, one of the basins with an intricate structure is elected for a thorough analysis of the system response dynamical pattern (periodic × chaotic), by means of Lyapunov exponent spectra, for specific initial displacement conditions associated to both rotating and non-rotating conditions.

Figure 2 shows a basin of attraction that will serve as a reference condition to be compared with further results obtained through parameters variation. The parameters used in this simulation are: $m_1 = m_2 = 1$ kg and $L_1 = L_2 = 1$ m and they were chosen in order to verify the numerical code implementation, by comparing with the results provided in both works conducted by Elinson (2013) and Small (2013). The results are displayed in a color scale that computes the necessary time (step iterations) for one of the pendula (either the internal or the external) to perform its first rotation. The dark red central region indicates non-rotating conditions, whereas the dark blue surrounding region is associated to fast rotating conditions. There are two points to be observed: a thin messy colored layer coating the dark red central region and some lamellas within the dark blue surrounding region. These features should be more deeply investigated, while varying the parameters.

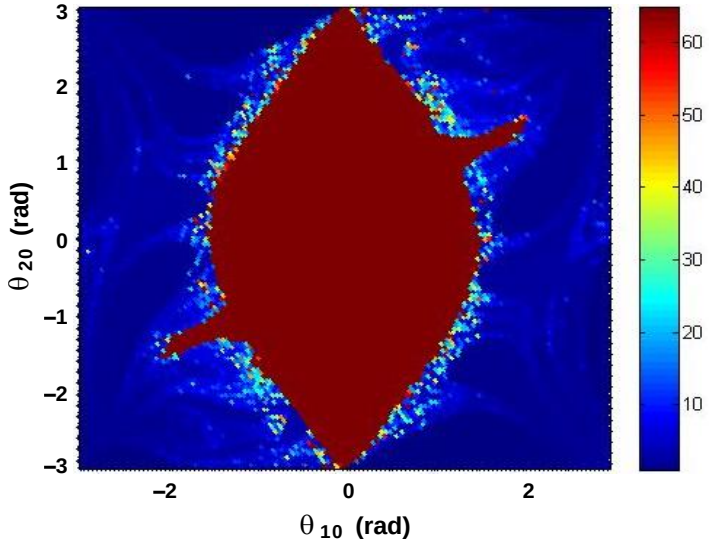

Figure 2 – Reference basin of attraction ($m_1 = m_2 = 1$ kg and $L_1 = L_2 = 1$ m).

Next, the kinetic energy is evaluated as a function of the initial displacements θ_{10} and θ_{20}, recalling that the initial velocities are null $\left(\dot{\theta}_{10} = \dot{\theta}_{20} = 0\right)$. This analysis is conducted as follows: for a fixed number of time iterations, for each set of initial conditions (only initial displacements), the velocities $\dot{\theta}_1$ and $\dot{\theta}_2$ are monitored along time. Then, average values for the kinetic energy of the system are obtained. This procedure is repeated iteratively in order to cover the desired range of initial conditions. After that, a kinetic energy surface is obtained as a function of the initial displacements.

Figure 3 presents the kinetic energy levels for the reference condition considered in Fig. 2 – i.e: $m_1 = m_2 = 1$ kg and $L_1 = L_2 = 1$ m. In Fig. 3a, clearly, the highest energy levels are concentrated in the corners. This is due to the fact that there is no external excitation and, thus, for the natural behavior, the greater the initial displacement conditions are, the greater the kinetic energy of the system is. Observing Fig. 3b, it is possible to identify a qualitative analogy with Fig. 2, where there is an increasing color gradient from center to corners.

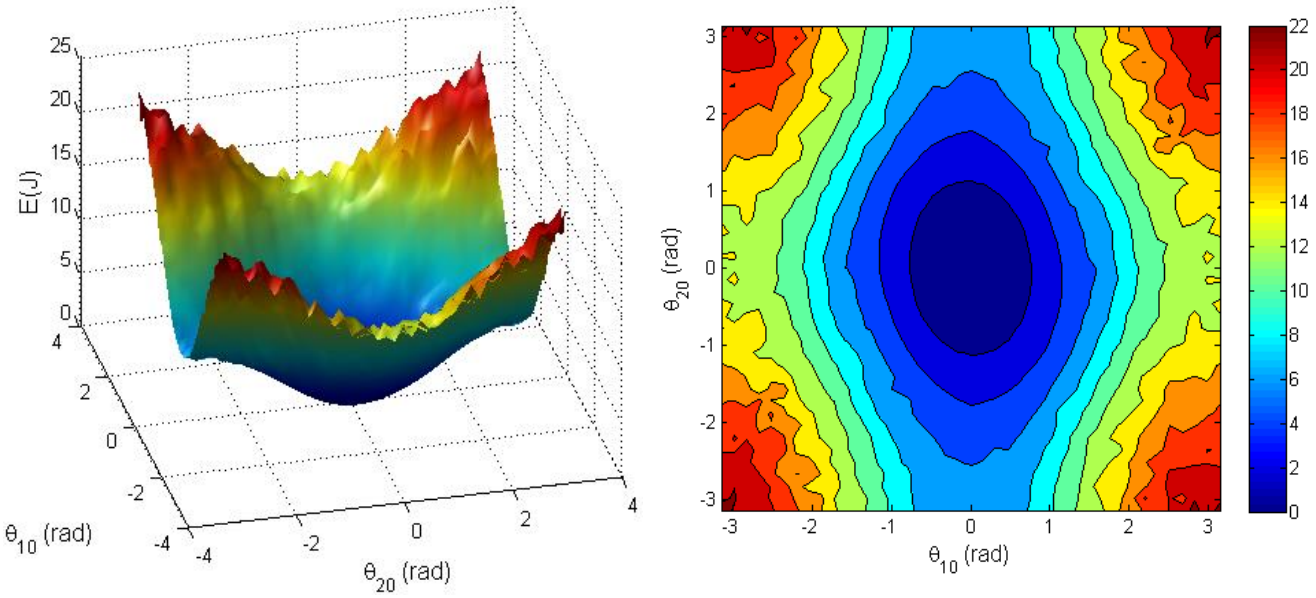

(a) (b)

Figure 3 – Kinetic energy analysis for the reference condition ($m_1 = m_2 = 1$ kg and $L_1 = L_2 = 1$ m).
(a) Kinetic energy surface as a function of the initial displacement conditions;
(b) Colormap projection of the kinetic energy surface.

Figure 4 presents the basin of attraction evolution, while varying the value of one specific parameter (m_1, m_2, L_1 or L_2), while the others are kept constant. As stated in the introduction, for an optimized energy harvesting, a stabilized rotating behavior is desirable (Nandakumar et al. 2012); therefore, this first analysis aims to identify two contrasting situations: the basin with the largest dark blue (rotating) region and the basin with the largest dark red (non-rotating) region.

In Fig. 4, while increasing the value of mass m_1 (Figs. 4a, 4b and 4c), there is a dark red region reduction that becomes vertically centered concentrated. Besides that, the lamellar structure present in the dark blue region becomes well-defined. The prominent nipples that take place in the northeastern and southwestern directions in Fig. 2 undergo a counterclockwise rotation. While reducing the value of mass m_1 (Fig. 4a) compared with the reference condition (Fig. 2), the outermost layer of the dark red region sprays out and the thin messy colored layer coating the dark red central region disappears.

While increasing the value of mass m_2 (Figs. 4d, 4e and 4f), the dark red region enlarges and sprays out, besides undergoing a clockwise rotation. The lamellar structure, together with the thin messy colored layer coating the dark red central region, gradually fades away.

Comparing the basin of attraction evolution for m_1 increasing (Figs. 4a, 4b and 4c) with the evolution for m_2 increasing (Figs. 4d, 4e and 4f), it is possible to notice that, if the ratio m_1/m_2 is preserved, the behavior remains the same (compare Fig. 4a with 4e and Fig. 4b with 4d). Besides that, when mass m_1 is grater than m_2, there is a reduction of the dark red non-rotating region.

While increasing the value of rod length L_1 (Figs. 4g, 4h and 4i), there is a dark red region reduction, which becomes vertically centered concentrated, besides a little clockwise rotation. The lamellar structure present in the dark blue region becomes more pronounced. The prominent nipples of Fig. 2 become bulky, until they are embodied by the dark red region. While reducing the value of length L_1 (Fig. 4g) compared with the reference condition (Fig. 2), the dark red region undergoes a horizontal enlargement.

While increasing the value of rod length L_2 (Figs. 4j, 4k and 41), there is a horizontal enlargement, accompanied by a vertical reduction, of the dark red region. The thin messy colored layer coating the dark red central region starts to escape from its surface, following the paths of the lamellar structure and forming dark red non-rotating isles. This behavior characterizes the basin of attraction erosion. The blue surrounding region becomes lighter, i.e.: for this region, the pendula take more time to rotate, compared with the reference condition (Fig. 2). While reducing the value of rod length L_2 (Fig. 4j), the dark red region becomes vertically centered concentrated. It is possible to infer that it is possible to rotate the dark red region by changing the value of rod length L_2.

Comparing the basin of attraction evolution for L_1 increasing (Figs. 4g, 4h and 4i) with the evolution for L_2 increasing (Figs. 4j, 4k and 41), again, it is possible to notice that, if the ratio L_1/L_2 is preserved, the behavior remains almost the same (compare Fig. 4g with 4k and Fig. 4h with 4j).

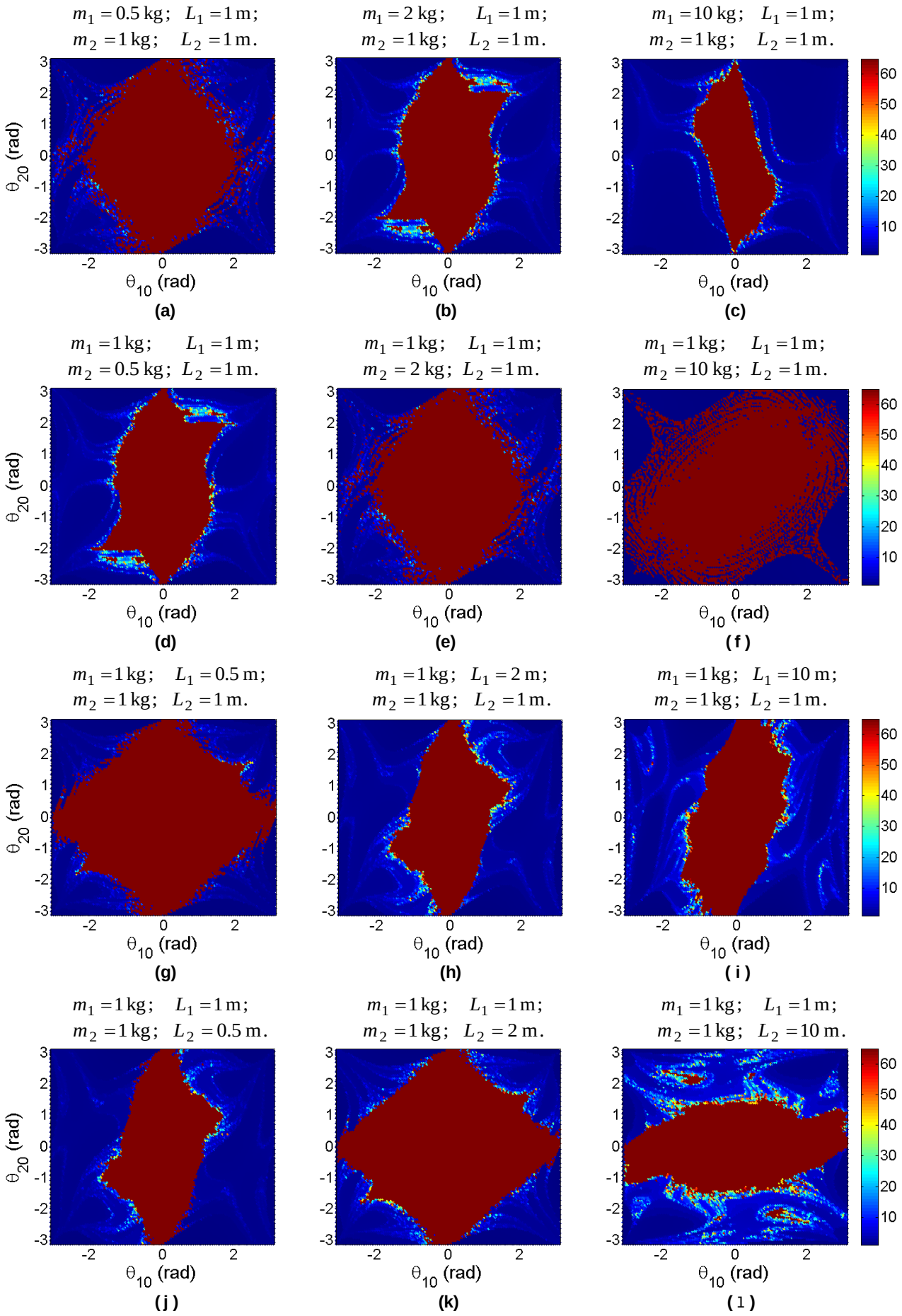

Figure 4 – Basins of attraction evolution varying the value of one specific parameter.

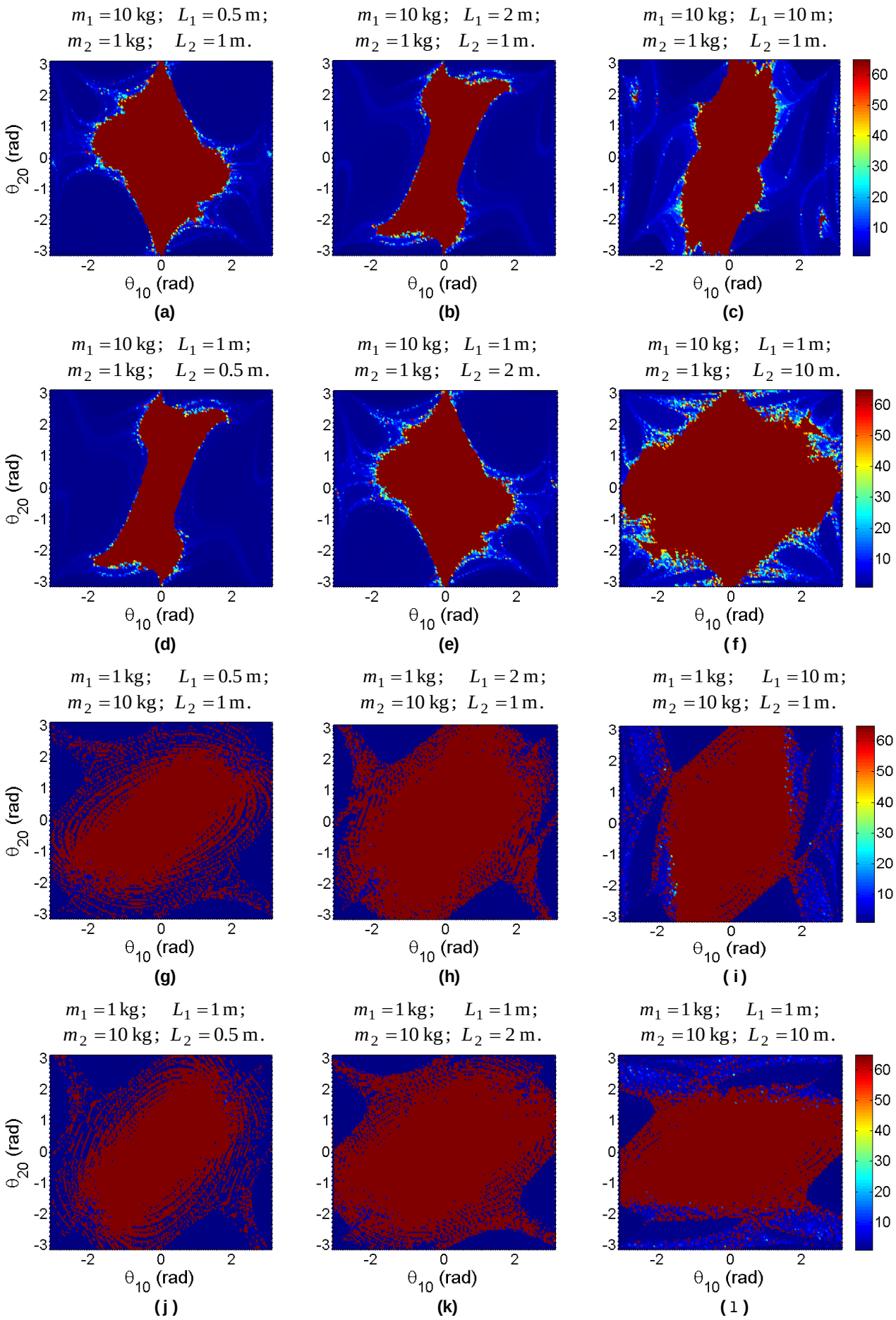

Figure 5 – Basins of attraction evolution simultaneously varying the value of two parameters.

Based on the analysis of the results provided in Fig. 4, it is possible to notice that, changes in the bob masses have a greater influence over the dark red region size than changes in the rod lengths. Thus, a second investigation, based upon two parameters variation, is conducted. This time, the parameters associated to both extreme situations identified in Fig. 4 are adopted, namely: the one that preferably favor the pendulum rotation, i.e. m_1 = 10 kg; m_2 = 1 kg (Fig. 4c – the narrowest dark red region) and for the one that preferably inhibit the pendulum rotation m_1 = 1 kg; m_2 = 10 kg (Fig. 4f – the largest dark red region). In the simulations of Fig. 5, the rod lengths are varied, considering these two fixed conditions for the bob masses.

Collectively analysing the results of Fig. 5, it is possible to notice that, while varying simultaneously two parameters, the obtained result may be understood as a combination of the single varied parameter responses. For instance, consider the result obtained in Fig. 5f, which may be viewed as a combination of Figs. 4c and 41. Nevertheless, none of the new simulated situations provide more extreme situations (narrowest/largest dark red central region) than those already obtained for the single varied parameter analysis (Figs. 4c and 4f). It is interesting to notice that, concerning the behavior maintenance, respecting the ratio L_1 / L_2, only in the case of m_1=10kg; m_2=1kg this behavior is observed (compare Fig. 5a with 5e and Fig. 5b with 5d). As a matter of fact, while comparing Fig. 4g with 4k and Fig. 4h with 4j, similar structures take place, with slight differences. Now, comparing Fig. 5g with 5k and Fig. 5h with 5j, the difference between them is coarser than the respective comparison in Fig. 4. Again in Fig. 5, as already found in Fig. 4, if mass m_1 is greater than m_2, there is a reduction of the dark red centered non-rotating region. Another point to be highlighted is that, for high values of mass m_2, both the lamellar structure and the thin messy colored layer coating the dark red central region of Fig. 2 disappear.

In the next analysis, the dynamical pattern (periodic × chaotic) of both rotating and non-rotating conditions is evaluated, by means of Lyapunov exponent spectra. Figure 6 reproduces an enlarged view of one of the previous basins of attraction that has an intricate structure (Fig. 41). Six initial displacement conditions are selected to be investigated – being four of them associated to rotating conditions (points ②,③,⑤,⑥) and two of them associated to non-rotating conditions (points ①,④). Initial velocity conditions are null.

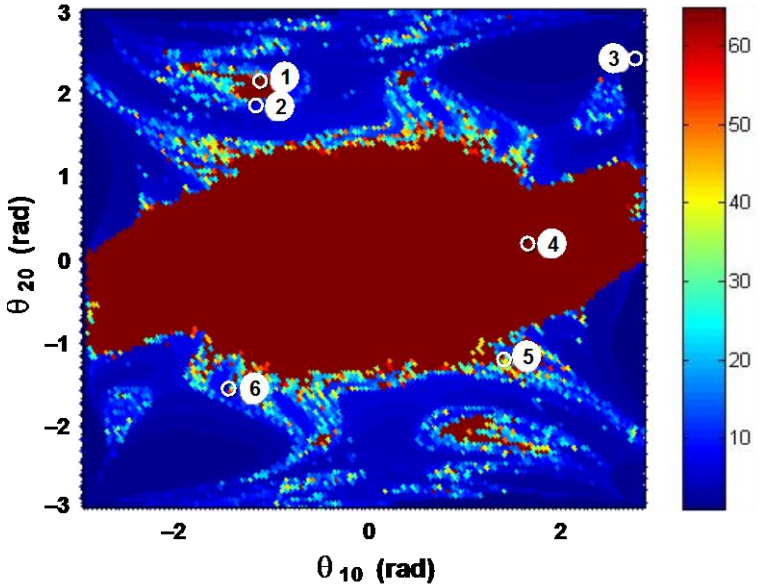

Figure 6 – Basin of attraction containing selected points for dynamical pattern analysis.

Figure 7 presents the Lyapunov spectra for the six selected points in Fig. 6. The converged exponent values are assigned in the figures captions.

Point ①, whose coordinates are: $(x; w) = (-1.143; 2.2)$, is located in a dark red isle. Figure 7a indicates all Lyapunov exponents null; thus, this pair of initial displacement conditions provides a periodic response.

Point ②, whose coordinates are: $(x; w) = (-1.194; 1.9)$, is located in a light blue region. Figure 7b indicates two Lyapunov exponents null and two of them real and symmetric; thus, this pair of initial displacement conditions provides a chaotic response (due to the positive Lyapunov exponent). Notice that the values displayed in this figure assign symmetric values for two of the exponents ($\lambda_1 = 0.30$ and $\lambda_4 = -0.30$). This feature is associated with the fact that the system is conservative and, thus, if there is an expansion in one direction (positive exponent), there is an equivalent contraction in another direction.

Point ③, whose coordinates are: $(x; w) = (3.041; 2.5)$, is located in a dark blue region. Figure 7c indicates, again, two Lyapunov exponents null and two of them real and symmetric; thus, this pair of initial displacement conditions provides a chaotic response.

Point ④, whose coordinates are: $(x; w) = (1.85; 0.15)$, is located in the dark red central region. Figure 7d indicates all Lyapunov exponents null; thus, this pair of initial displacement conditions provides a periodic response.

Point ⑤, whose coordinates are: $(x; w) = (1.598; -1.283)$, is a yellow point belonging to the thin messy colored layer coating the dark red central region. Figure 7e indicates, one more time, two Lyapunov exponents null and two of them real and symmetric; thus, this pair of initial displacement conditions provides a chaotic response.

Point ⑥, whose coordinates are: $(x; w) = (-1.486; -1.683)$, is an orange point belonging to the thin messy colored layer coating the dark red central region. Figure 7e indicates, one more time, two Lyapunov exponents null and two of them real and symmetric; thus, this pair of initial displacement conditions provides a chaotic response.

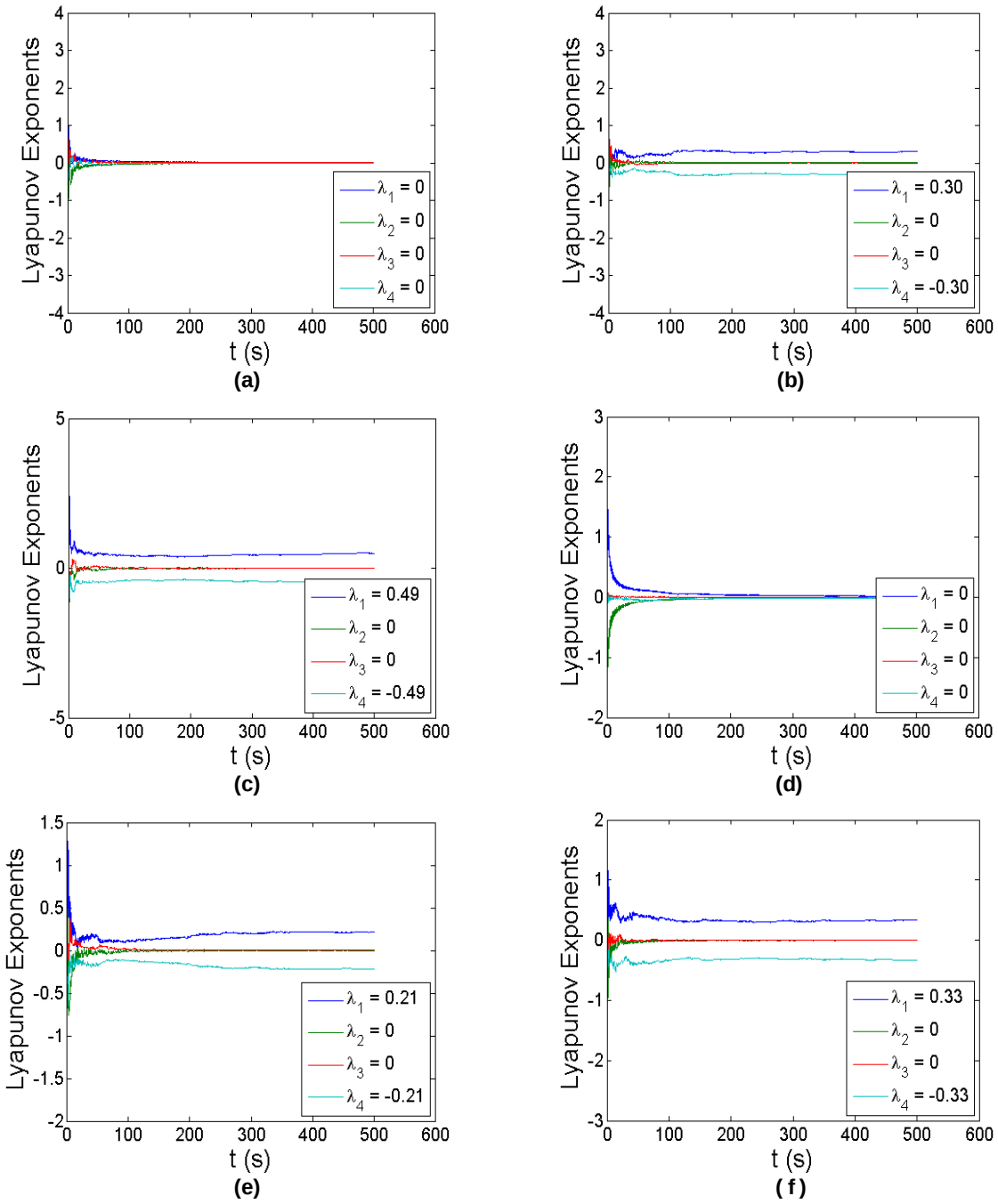

Figure 7 – Lyapunov exponents for selected points for dynamical pattern analysis.

CONCLUDING REMARKS

This paper discusses the dynamycal analysis of a double pendulum, distinguishing rotating from non-rotating conditions. Basins of attraction are plotted, for the conservative behavior, mapping the initial displacement conditions, for different parameter values. It is found that, changes in the bob masses are adequate to control the size of the non-rotating region, such that m_1 grater than m_2 enables a reduction of the non-rotating region; while changes in the rod lengths are adequate to control the position of the non-rotating region, especially the external pendulum rod length. Moreover, the *Lyapunov* exponent analysis suggests that, whenever one of the pendula rotates, a chaotic motion takes place; on the other hand, non-rotating conditions are supposed to be associated to periodic/quasi-periodic behaviors. This study is a first approach towards energy harvesting modeling. For a feasible energy harvester, it is necessary to extract energy from an external source; thus, the forced response is the one of specific interest. The present contribution suggests optimal parameters for maximizing the rotating region, concerning the natural behavior. Intuitively, these parameters should be the starting point for a further work on energy harvesting.

ACKNOWLEDGMENT

The authors would like to acknowledge the support of the Brazilian Research Agencies CNPq, CAPES, FAPERJ as well as INCT-EIE (National Institute of Science and Technology - Smart Structures in Engineering). The acknowledgement also applies to Air Force Office of Scientific Research (AFOSR).

REFERENCES

Abrams, D.M. & Strogatz, S.H.; 2004; “Chimera States for Coupled Oscillators”; Physical Review Letters; Vol. 93; N. 17; Article ID 174102; 4 pp.

Abrams, D.M. & Strogatz, S.H.; 2006; “Chimera States in a Ring of Nonlocally Coupled Oscillators”; International Journal of Bifurcation and Chaos; Vol. 16; N. 1; pp. 21–37

Awrejcewicz, J.; 1991; “Bifurcation and Chaos in Coupled Oscillators”; World Scientific Pub Co; 250 pp.

Bishop, S.R. & Xu, D.L.; 1997; “Control of the Parametrically Excited Pendulum”; IUTAM Symposium on Interaction between Dynamics and Control in Advanced Mechanical Systems (Volume 52 of the series Solid Mechanics and Its Applications); Ed. Springer; pp. 43–50.

Bishop, S.R.; Xu, D.L. & Clifford, M.J.; 1996; “Flexible Control of the Parametrically Excited Pendulum”; Proceedings of The Royal Society A; Vol. 452; N. 1951; pp. 1789–1806.

Buskirk, R.V. & Jefries, C.; 1985; “Observation of Chaotic Dynamics of Coupled Nonlinear Oscillators”; Physical Review A; Vol. 31; N. 5; pp. 3332–3357.

Cross, R.; 2005; “A Double Pendulum Swing Experiment: in Search of a Better Bat”; American Journal of Physics; Vol.73; pp. 330–339.

Cross, R.; 2011; “A Double Pendulum Model of Tennis Strokes”; American Journal of Physics; Vol. 79; pp. 470–476.

De Paula, A.S.; Savi, M.A.; Wiercigroch, M. & Pavlovskaia, E.; 2012; “Bifurcation Control of a Parametric Pendulum”; International Journal of Bifurcation and Chaos; Vol. 22; N. 5; 14 pp.

De Paula, A.S.; Savi, M.A.; Vaziri, V.; Pavlovskaia, E. & Wiercigroch, M.; 2015; “Experimental Bifurcation Control of a Parametric Pendulum”; Journal of Vibration and Control; pp. 1–13.

Elinson, J.; 2013; “Nonlinear Dynamical Systems”; Edited by: Chasnov, J.R. – Department of Mathematics – Harvey Mudd College; pp. 16–23.

Heyl, J.S.; 2008; “The Double Pendulum Fractal”; Department of Physics and Astronomy; University of British Columbia, 8 pp.

Santos, I.F.; “Dinâmica de Sistemas Mecânicos”; Ed. Makron Books; 2001.

Ivancevic, V.G. & Ivancevic, T.T.; 2007; “High-dimensional Chaotic and Attractor Systems: A Comprehensive Introduction”; Ed. Springer; 700 pp.

Kapitaniak, T.; 2003; “Chaotic Oscillations in Higher-Dimensional Systems”; Special issue of Chaos, Solitons and Fractals; Vol. 15, N. 2.

Kapitaniak, T. Kuzma, P.; Wojewoda, J.; Czolczynski, K. & Maistrenko, Y.; 2014; “Imperfect Chimera States for Coupled Pendula”; Scientific Reports 4, Article ID 6379; 4 pp.

Lai, Y.C. & Grebogi, C.; 1999; “Modeling of Coupled Chaotic Oscillators”. Physical Review Letters; Vol. 82; N. 24; pp. 4803–4806.

Lankalapalli, S. & Ghosal, A., 1997, “Chaos in Robot Control Equations”, International Journal of Bifurcation and Chaos, Vol. 7, pp. 707–720.

Lenci, S.; Pavlovskaia, E.; Rega, G. & Wiercigroch, M.; 2008; “Rotating Solutions and Stability of Parametric Pendulum by Perturbation Method”; Journal of Sound and Vibration; Vol. 310; pp. 243–259.

Machado, L.G.; Savi, M.A. & Pacheco, P.M.L.C.; 2003; "Nonlinear Dynamics and Chaos in Coupled Shape Memory Oscillators"; International Journal of Solids and Structures; Vol. 40; N. 19; pp. 5139–5156.

Marszal, M.; Jankowski, K.; Perlikowski, P. & Kapitaniak, T.; 2014; "Bifurcations of Oscillatory and Rotational Solutions of Double Pendulum with Parametric Vertical Excitation"; Mathematical Problems in Engineering; Vol. 2014.

Martens, E.A.; Panaggio, M.J. & Abrams, D.M.; 2016; "Basins of Attraction for Chimera States"; New Journal of Physics; Vol. 18; Article ID 022002; 20 pp.

Nandakumar, K.; Wiercigroch, M. & Chatterjee, A.; 2012; "Optimum Energy Extraction from Rotational Motion in a Parametrically Excited Pendulum"; Mechanics Research Communications; Vol. 43; pp. 7–14.

Najdecka, A; Narayanan, S. & Wiercigroch, M.; 2015; "Rotary Motion of the Parametric and Planar Pendulum under Stochastic Wave Excitation"; International Journal of Non-Linear Mechanics; Vol. 71; pp. 30–38.

Rafat, M.Z.; Whealand, M.S. & Bedding, T.R.; 2009; "Dynamics of a Double Pendulum with Distributed Mass"; American Journal of Physics; Vol. 77; N. 3; 20 pp.

Raj, S.P.; Rajasekar S. & Murali, K.; 1999; "Coexisting Chaotic Attractors, their Basin of Attractions and Synchronization of Chaos in Two Coupled Duffing Oscillators"; Physics Letters A; Vol. 264; N. 4; pp. 283–288.

Sabarathinama, S.; Thamilmaran, K.; Borkowski, L.; Perlikowski, P.; Brzeski, P.; Stefanski, A. & Kapitaniak, T.; 2013; "Transient Chaos in Two Coupled, Dissipatively Perturbed Hamiltonian Duffing Oscillators"; Communications in Nonlinear Science and Numerical Simulation; Vol. 18; N. 11; pp. 3098–3107.

Shibata, H.; 1998; "Quantitative Characterization of Spatiotemporal Chaos"; Physica A; Vol. 252; pp. 428–449.

Shinbrot, T., Grebogi, C., Wisdom, J. & Yorke, J.A.; 1992; "Chaos in a Double Pendulum"; American Journal of Physics; Vol. 60; N.6; pp. 491–499.Lankalapalli, S. & Ghosal, A.; 1997; "Chaos in Robot Control Equations"; International Journal of Bifurcation and Chaos, Vol.7; pp. 707–720.

Small, A.; 2013; "One Signature of Chaosin the Double Pendulum"; Department of Physics and Astronomy – California State Polytechnic University; 16 pp.

Stachowiak, T. & Okada, T.; 2006; "A Numerical Analysis of Chaos in the Double Pendulum"; Chaos, Solitons and Fractals; Vol. 29, pp. 417–422.

Strogatz, S.H.; Marcus, C.M.; Westervelt, R.M. & Mirollo, R.E.; 1989; "Collective Dynamics of Coupled Oscillators with Random Pinning"; Physica D: Nonlinear Phenomena; Vol. 36; N. 1-2; pp. 23–50.

Szuminski, W.; 2014; "Dynamics of Multiple Pendula Without Gravity"; Chaotic Modeling and Simulation; Vol. 1; pp. 57–67.

Tang, Y.; Groninger, E.; Foster, B.; Aliaga, D.; Buresh, T.R. & Madsen; M.J.; 2011; "Chaos of the Double Pendulum"; Wabash Journal of Physics; Vol. 2.3; pp.1–8.

Ulrichs, H.; Mann, A. & Parlitz, U.; 2009; "Synchronization and Chaotic Dynamics of Coupled Mechanical Metronomes"; Chaos: An Interdisciplinary Journal of Nonlinear Science; Vol. 19; N. 4; Article ID 043120; 6 pp.

Umberger, D.K.; Grebogi, C.; Ott, E. & Afeyan, B.; 1989; "Spatiotemporal Dynamics in a Dispersively Coupled Chain of Nonlinear Oscillators"; Physical Review A; Vol. 39; N. 9; pp. 4835–4842.

Vincent, U.E. & Kenfack, A.; 2008; "Synchronization and Bifurcation Structures in Coupled Periodically Forced Non-identical Duffing Oscillators"; Physica Scripta; Vol. 77, N. 4; Article ID 045005.

RESPONSIBILITY NOTICE

The authors are the only responsible for the printed material included in this paper.